Doping dependence of vortex regimes in $Y_{1-x}Pr_xBa_2Cu_3O_{7-\delta}$ single crystals

P. Gyawali, V. Sandu,* and C. C. Almasan
Department of Physics, Kent State University, Kent, Ohio 44242, USA

B. J. Taylor and M. B. Maple
Department of Physics, University of California at San Diego, La Jolla, California 92903, USA
(Received 8 February 2007; revised manuscript received 17 August 2007; published 6 May 2008)

Magnetic relaxation measurements on a series of $Y_{1-x}Pr_xBa_2Cu_3O_{7-\delta}$ ($x=0.13$, 0.34, and 0.47) single crystals were performed over a large field and temperature range in order to investigate the characteristics of the vortex matter across the second magnetization peak (SMP). The magnitude of the SMP varies nonmonotonically with Pr concentration, i.e., the irreversible magnetization normalized by its value at the onset field H_{on} displays a maximum for the $x=0.34$ single crystal. The two characteristic fields, H_{on} and H_{sp}, follow different temperature T dependences: $H_{on} \propto T^{\nu_{on}}$ and $H_{sp} \propto [1-(T/T_c)^2]^{\nu_{sp}}$. The extracted values of the apparent activation energy U^* and the creep exponent μ display a maximum at a field $H_{on} < H^* < H_{sp}$. Their field dependences point toward the coexistence of both elastic and plastic creep for $H > H_{on}$. The degree of participation of each creep mechanism is determined by the charge carrier density, which controls both the elastic properties of the vortex matter and the pinning potential.

DOI: 10.1103/PhysRevB.77.174504 PACS number(s): 74.25.Ha, 74.25.Qt, 74.72.Bk

I. INTRODUCTION

One of the most challenging manifestations of the vortex matter in cuprate superconductors is the second magnetization peak (SMP) or fishtail displayed in the isothermal magnetization at an intermediate magnetic field H_{sp} much lower than the irreversibility field.[1–11] Theoretically, it has been shown that at this field, the flux line lattice crosses over from a dislocation-free Bragg glass structure present at low magnetic fields, which has an algebraic decay of translational correlations, to a vortex glass.[12–14] The existence of this order-disorder transition was later observed experimentally.[3,15,16] The magnetic field increases the entropy of the flux-line system[17] beyond that introduced by the quenched disorder. Additionally, the field triggers the competition between the elastic U_{el} and pinning U_{pin} energies at constant temperature (see, for example, Ref. 18). At low fields, the weak point disorder is important and the flux lines form an elastic quasiordered dislocation-free lattice. As the field increases, the elastic screening length,[19] hence the interlayer interaction, decreases, which weakens the elastic response of the lattice and facilitates the invasion of topological defects (dislocations). The break of the long range order allows a better matching of the vortex lines to the pinning potential and, consequently, enhances the irreversibility present in magnetization. This effect starts at the onset field H_{on}. Above this field, the vortex matter, which is assumed to be a lattice, displays a granular structure, namely, a network of dislocations that separate grains of vortex matter that still retain a higher elasticity.[20,21] The dislocation lines obey a characteristic dynamics including pinning and depinning processes.[22] Direct evidence for such a proposal has been obtained from muon-spin rotation experiments.[23,24]

Although such a behavior is universal, each class of cuprates shows a specific behavior, in which the second magnetization peak is more or less pronounced, depending on the relative values of the elastic and pinning energies, which, in turn, along with the characteristic lengths (elastic screening length L_0 and Larkin length) depend on the superfluid density n_s (through the magnetic penetration length λ because the effective mass is almost n_s independent),[25] anisotropy γ, and the disorder parameter δ_{dis}.[19,26–28] Usually, in the absence of a special treatment, e.g., particle irradiation, weak disorder due to oxygen vacancies is always present in cuprates. In $YBa_2Cu_3O_{7-\delta}$, charge underdoping is obtained by oxygen removal from the Cu(1)-O(1) chains. This procedure also induces disorder consisting in different sequences of full Cu-O(1) and empty Cu(1) chains and an increased occupation of O(5) sites.[29] A second consequence of the underdoping is the fast increase in the anisotropy. Thus, the three parameters n_s, γ, and δ_{dis} are interconnected in a complex way. This makes it difficult to systematically study the effect of one of these material parameters on the evolution of the vortex matter from a quasiordered Bragg glass to a disordered amorphous or liquid state (see, for example, Ref. 30).

It is possible to reduce the number of the above mentioned parameters from three to two by applying a doping method that practically does not introduce any additional effective disorder. This is the case of Pr substitution for Y in $YBa_2Cu_3O_{7-\delta}$. The density of free charge carriers is extremely sensitive to Pr even at optimal oxygenation due to carrier localization in the Fehrenbacher-Rice band as a result of Pr-O hybridization,[31,32] while the disorder created by the Pr ions is less effective to pinning compared to oxygen.[33] It is remarkable that the integrity of the chains, hence the orthorhombicity, is preserved in this material, notwithstanding the change in the charge carrier density. So, the main source of the weak pinning, i.e., oxygen disorder, is maintained almost constant. The only effect of Pr on the pinning parameter results from its dependence on the magnetic penetration length.[18,26] In addition, it has been found experimentally that the anisotropy $\gamma \equiv \sqrt{\rho_c/\rho_{ab}}$, as obtained from transport measurements, changes nonmonotonically with doping and, hence, charge carrier density.[34] Specifically, it increases fast up to $\gamma=24$ at $x=0.13$, then it stays almost constant up to $x=0.42$, and decreases abruptly to $\gamma=9$ in the vicinity of

the superconductor-insulator transition ($x=0.53$). However, since the increase (decrease) in the anisotropy decreases (increases) all of the energy scales involved in the equilibrium of the flux-line system, we expect only a marginal effect of this parameter in what follows. Therefore, the Pr substitution for Y in $YBa_2Cu_3O_{7-\delta}$ facilitates the investigation of the effect of the superfluid density on the evolution and crossovers of different regimes of the vortex matter.

In this paper, we explore the evolution of the vortex matter state in the temperature and field ranges where the SMP is present by studying the magnetization and magnetic relaxation of a series of $Y_{1-x}Pr_xBa_2Cu_3O_{7-\delta}$ single crystals. Our study has shown that the main ingredient that controls the evolution of the vortex matter through the different regimes is the charge carrier density. The SMP is first enhanced and then suppressed as x increases. The reason for this behavior is the softening of the elastic moduli, which makes the vortex lattice less stable to defect invasion.

II. EXPERIMENTAL DETAILS

A series of $Y_{1-x}Pr_xBa_2Cu_3O_{7-\delta}$ ($x=0.13$, 0.34, and 0.47) single crystals was chosen to perform extensive magnetization measurements. The three single crystals for which data are presented here are platelets of sizes $1.25\times0.95\times0.12$, $0.75\times0.4\times0.1$, and $0.83\times0.47\times0.03$ mm^3 with critical temperatures T_c of 82, 50, and 34 K, respectively. Details of the crystal growth are reported elsewhere.[35] For completeness, we also show the data for two $x=0$ single crystals, one with size $3.3\times2.4\times1.1$ mm^3 taken from Ref. 36 and another one with size $1.15\times1.11\times0.035$ mm^3, as taken from Ref. 37.

Magnetic field H dependent magnetization M and relaxation measurements were performed at different temperatures T in the reduced temperature T/T_c range between 0.2 and 0.9 by using a Quantum Design superconducting quantum interference device magnetometer with the external magnetic field applied parallel to the c axis of the single crystal. We used the persistent current mode with a scan length of 40 mm, which guarantees an excellent magnetic field homogeneity. The single crystals were cooled in zero field to the desired temperature and the whole $M(H)$ loop was recorded in increasing and then decreasing field with H steps chosen to get the finest details in $M(H)$. After performing a hysteresis loop at a given temperature, the sample was warmed up to $T\gg T_c$ and cooled in zero field to the next set temperature.

For all of the single crystals studied, the demagnetization factor D, which was calculated from the initial slope of the virgin hysteresis curves, was found to be higher than 0.9; hence, the magnetic induction $B=H+4\pi(1-D)M\approx H$. Therefore, we have used the magnetic field H throughout this paper instead of the magnetic induction B.

Magnetic relaxation was measured in the normal dc mode by monitoring the time decay of the magnetic moment. For these measurements, we cooled the single crystal to the desired temperature in zero field, the magnetic field was then ramped to the target value, and the magnetization was recorded as a function of time t every 175 s for about 2 h.

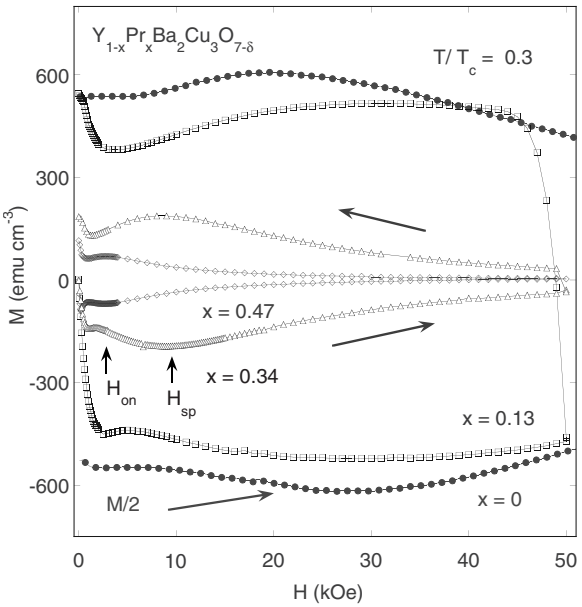

FIG. 1. Magnetic hysteresis loops for $Y_{1-x}Pr_xBa_2Cu_3O_{7-\delta}$, $x=0$ (Ref. 35), 0.13, 0.34, and 0.47 single crystals, measured at the same reduced temperature $T/T_c\approx0.3$. The arrows indicate the position of the onset H_{on} and second magnetization peak H_{sp} fields.

III. RESULTS AND DISCUSSION

Figure 1 shows the magnetization loops $M(H)$ for three Pr concentrations measured at $T/T_c\approx0.3$. For completeness, we also show the $M(H)$ data for an $x=0$ single crystal taken from Ref. 36. All of these four $M(H)$ curves are almost symmetric around the $M=0$ axis, i.e., the reversible magnetization is nearly zero, and they display a similar field dependence. Specifically, the absolute value of the magnetization decreases with increasing field beyond the full penetration field, reaches a minimum at the onset field H_{on}, then increases again and reaches a SMP at H_{sp}, and, finally, decreases to zero with a further increase of the magnetic field. Previously, both H_{on} and H_{sp} have been related to the order-disorder transition from a dislocation-free Bragg glass to a disordered vortex matter with a glassy structure. For example, several theoretical studies take the peak field H_{sp} as the order-disorder line,[12,13,27,28] while in experimental studies of $YBa_2Cu_3O_{7-\delta}$, the order-disorder crossover has been taken either as the kink observed for $H_{on}<H<H_{sp}$ (Refs. 15 and 37) or at H_{on} (Refs. 3 and 38).

The goal of the present work is to study the effect of charge carrier density n_s on the evolution of the vortex matter in the temperature and field ranges where the SMP is present. A specific vortex state at a fixed T and H is determined by an n_s-dependent interplay between the pinning landscape and the parameters that govern the stability of the vortex lattice, namely, disorder, critical current density J_c, and elastic moduli. The study of Pr-doped $YBa_2Cu_3O_{7-\delta}$ ensures that Pr doping does not change the disorder but only decreases n_s. Hence, by studying this system, one studies the above mentioned interplay only as a function of n_s. The decrease of J_c with decreasing n_s is reflected in the continuous decrease in the irreversible magnetization, including its value

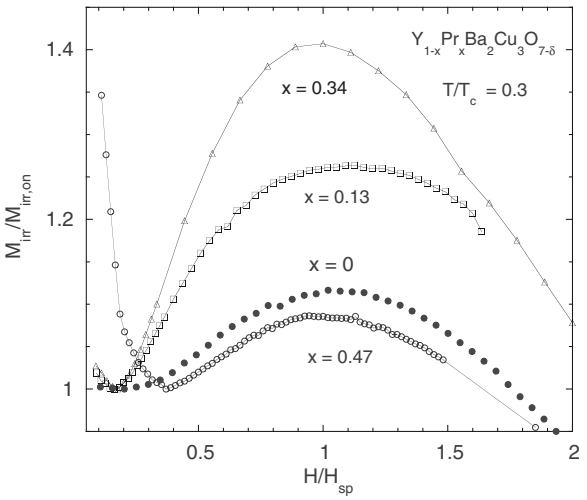

FIG. 2. Plot of the irreversible magnetization M_{irr} normalized to its value $M_{irr,on}$ at the onset of the second magnetization peak as a function of the reduced field H/H_{sp} for $Y_{1-x}Pr_xBa_2Cu_3O_{7-\delta}$, $x=0$ (Ref. 35), 0.13, 0.34, and 0.47 single crystals, measured at the same reduced temperature $T/T_c \approx 0.3$. Inset: x dependence of the absolute value of the irreversible magnetization at the second magnetization peak $M_{irr,sp}$ measured at the same reduced temperature.

at the SMP, with decreasing n_s, i.e., increasing x (see Fig. 1). Hence, a plot of $M_{irr}/M_{irr,on}$, the irreversible magnetization $M_{irr} \equiv (M^- - M^+)/2$ (M^+ and M^- are the magnetizations measured in increasing and decreasing magnetic field, respectively) normalized by the value of the magnetization at the onset field $M_{irr,on}$, vs H/H_{sp} eliminates the effect of $J_c(n_s)$. Therefore, such a plot reflects, at constant H, only the n_s-dependent interplay between the pinning landscape and the elastic moduli, while it reflects the interplay between the pinning landscape and the H-induced disorder at constant doping x.

Figure 2 is a plot of $M_{irr}/M_{irr,on}$ vs H/H_{sp} for three different Pr dopings as well as for an $x=0$ single crystal taken from Ref. 36, all measured at a reduced temperature $T/T_c \approx 0.3$. The normalized irreversible magnetization in the SMP region displays a conspicuous nonmonotonic behavior as a function of the charge carrier density, i.e., it increases with decreasing charge carrier density down to $n_s=0.083$ ($x=0.34$) followed by a decrease for even lower n_s (higher Pr concentrations). In fact, our magnetic investigations of the $x=0.53$ single crystals have shown that the SMP is absent at this Pr concentration.[39]

The SMP dynamics is usually also size dependent. Specifically, it has been shown experimentally that the reduction of the sample size produces the vanishing of the SMP[40,41] and the shift of the order-disorder transition field to higher temperatures.[42] However, the fact that the maximum peak effect in Fig. 2 takes place in the narrowest single crystal studied ($x=0.34$) shows that the size effect reported previously does not change the observed nonmonotonic behavior of the normalized irreversible magnetization. Nevertheless, it could be responsible for the precise location of the second magnetization peak.

The nonmonotonic behavior of $M_{irr}/M_{irr,on}$ vs H/H_{sp} can be explained as follows: the elastic moduli C_{44} and C_{66} decrease with decreasing charge carrier density n_s (increasing x).[26] The decrease in the elastic moduli reduces the energy scale of the dislocations[22] [$E_D=(C_{44}C_{66})^{1/2}b/4\pi$, where b is the Burger's vector], which makes their generation easier and, subsequently, allows a better matching of the flux-line system to the n_s-dependent pinning landscape. Therefore, at high charge carrier densities (e.g., the $x=0$ or 0.13 single crystal), the flux-line system is rather stiff since the creation of dislocations requires a rather high energy. Hence, the density of dislocations is rather low and their relative contribution to the total irreversibility, i.e., pinning of the flux lines, though important, is not substantial. At low charge carrier densities (e.g., the $x \sim 0.47$ single crystal), the flux-line system is soft since dislocations are easily created (C_{44} and C_{66} are small, hence E_D is low). Nevertheless, despite the increased plasticity of the flux-line system due to the increased number of dislocations, the values of $M_{irr}/M_{irr,on}$ are smaller than the ones for the low Pr doping (high n_s) case due to the net decrease in the strength of the n_s-dependent pinning landscape. However, there is an optimum charge carrier density (e.g., the $x \sim 0.34$ single crystal) for which the softening of the flux lattice due to the decrease in the elastic moduli allows the optimum matching of the flux-line system to the pinning landscape, maximizing the irreversible magnetization $M_{irr}/M_{irr,on}$.

The H dependence of $M_{irr}/M_{irr,on}$ for a constant x displays a broad maximum around the field H_{sp} corresponding to the second magnetization peak. This suggests that the gradual process of field driven disordering gives rise to a continuous increase in the density of dislocation loops. Additional disorder (transient disorder) is also injected into the sample through inhomogeneous surface barriers[43,44] and its lifetime increases as the field approaches the order-disorder transition field. Hence, elastic and plastic behaviors coexist in different degrees over a large field range starting at H_{on} (below which only elastic creep is present[3]) and ending well above H_{sp}, with the elastic behavior dominant for $H<H_{sp}$ and plastic behavior prevailing for $H>H_{sp}$. This result is supported by scanning tunneling microscopy investigations,[16] which have shown the presence of dislocations even near H_{on}, and by neutron scattering data, which have shown surviving Bragg peaks far above H_{sp}.[45] Note that numerical simulations have shown that homogeneous flux-line domains, i.e., systems displaying elastic creep, survive up to $0.8H_{c2}$.[46]

The overall behavior discussed above is present over the whole temperature range $0.3 \leq T/T_c \leq 0.9$. As the temperature increases, both characteristic fields H_{on} and H_{sp} shift to lower values, but they follow different T dependences, namely, $H_{on} \propto T^{-\nu_{on}}$ (see inset of Fig. 3) while $H_{sp} \propto [1-(T/T_c)^2]^{\nu_{sp}}$ (see Fig. 3), with $\nu_{on}=1.13$, 1.9, 2.1, and 1.99, and $\nu_{sp}=1.36$, 2.02, 2.53, and 2.23 for the $x=0$ (Ref. 37), 0.13, 0.34, and 0.47 single crystal, respectively.

The $H_{sp}(T)$ of the present study does not show the upturn at high temperatures reported for optimally doped $YBa_2Cu_3O_{7-\delta}$.[6,8,15,47] Nevertheless, previous measurements have shown that the $H_{sp}(T)$ behavior is extremely sensitive to small deviations from optimal doping[6,47] and that the suppression of the high temperature upturn for $YBa_2Cu_3O_{7-\delta}$ occurs for $\delta \geq 0.06$. On the other hand, disorder introduced

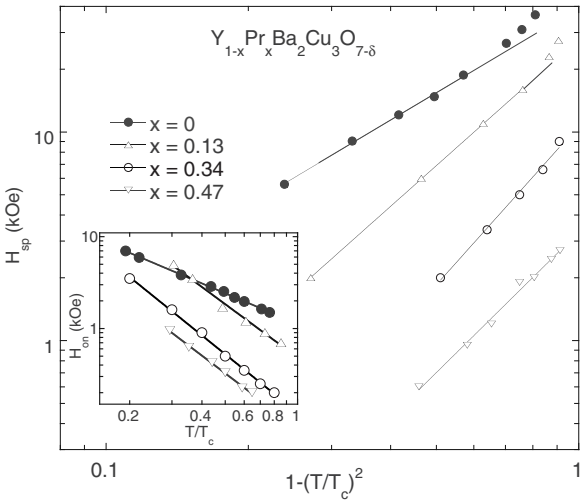

FIG. 3. Log-log plot of the second magnetization peak H_{sp} vs reduced temperature T/T_c for $Y_{1-x}Pr_xBa_2Cu_3O_{7-\delta}$, $x=0$ (Ref. 36), 0.13, 0.34, and 0.47 single crystals. Inset: Log-log plot of the onset field H_{on} vs T/T_c for the same single crystals.

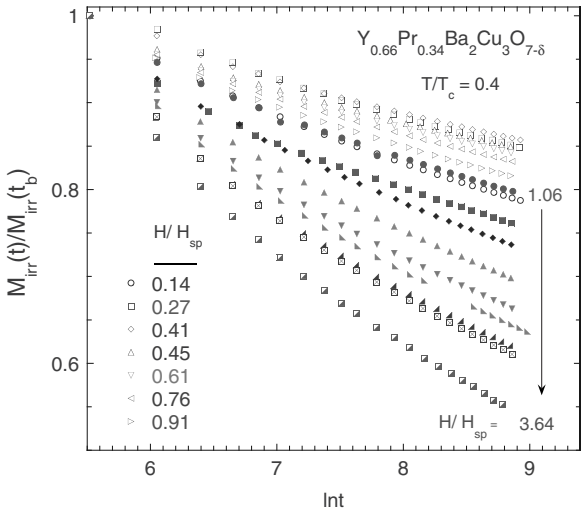

FIG. 4. Logarithm of time t evolution of the irreversible magnetization M_{irr} of an $Y_{0.66}Pr_{0.34}Ba_2Cu_3O_{7-\delta}$ single crystal measured at the reduced temperature $T/T_c=0.4$ and for different field values around the second magnetization peak. Open symbols below H_{sp} and partially filled or close symbols above H_{sp} represent 1.06, 1.21, 1.51, 1.82, 2.12, 2.42, 2.73, 2.03, and 3.64 as shown by the arrow.

by electron irradiation was found to decrease, but not suppress, the high temperature upturn of $H_{sp}(T)$ even for a fluence as high as 2×10^{18} cm^{-2}.[48] Therefore, we conclude that the reduction of the charge carrier density by Pr substitution for Y gives rise to the suppression of the upturn in $H_{sp}(T)$ at high T, and, hence, the monotonic decrease of H_{sp} with increasing T. Specifically, the decrease in the superfluid density n_s with increasing doping x increases the magnetic penetration length λ at high T, and, hence, decreases H_{sp} [$H_{sp}\propto 1/\lambda^4$ (Ref. 2)]. Notice that the x dependence of the exponent ν_{sp} shows a similar nonmonotonic trend as the SMP itself. Finally, we do not rule out an additional effect of the transient disorder, which is more effective in the narrower samples (x=0.34 and 0.47), in the precise determination of the H_{sp} position,[42,44] mainly at low temperatures, where the annealing processes are slower.

We also performed magnetization relaxation measurements on $Y_{1-x}Pr_xBa_2Cu_3O_{7-\delta}$ at different fields and temperatures around the SMP in order to further study the evolution of the vortex matter with the charge carrier density. Figure 4 is a plot of the time t dependence of the irreversible magnetization M_{irr} normalized by the first measured magnetization $M_{irr}(t_b)$ ($t_b\sim250$ s) for the x=0.34 single crystal measured at a reduced temperature T/T_c=0.4 and different reduced magnetic fields H/H_{sp} both below and above H_{sp}. We obtained $M_{irr}(t)$ by subtracting the reversible magnetization, extracted from the $M(H)$ loops (see Fig. 1), from the measured magnetization. The data of Fig. 4 are representative of all of the single crystals measured. It is salient that the data do not follow a logarithmic t dependence. Hence, we analyzed these data in the framework of the collective creep theory in which[49]

$$M_{irr}(t,T,H)=M_{irr}(t_0,T,H)\left[1+\frac{\mu k_BT}{U_0(H)}\ln\left(\frac{t}{t_0}\right)\right]^{-1/\mu}, \quad (1)$$

where U_0 is the effective pinning potential, t_0 is a macroscopic quantity depending on the sample size and it should not be confused with the actual microscopic attempt time,[49] and μ is the collective creep exponent. The normalized relaxation rate S is obtained from Eq. (1) as

$$S(J,T,H)\equiv-\frac{1}{M_{irr}(t)}\frac{dM_{irr}(t)}{d\ln(t)}=\frac{k_BT}{U^*(J,T,H)}, \quad (2)$$

where

$$U^*(J,T,H)\equiv U_0+\mu k_BT\ln\left(\frac{t}{t_0}\right) \quad (3)$$

is the apparent activation energy, which is larger than U_0 due to current relaxation. Note that, for convenience, we define S as a positive quantity. One can experimentally determine U^* from Eq. (2) with the normalized relaxation rate S obtained from the data of Fig. 4. In doing so, the relaxation rate is normalized to the initial magnetization $M_{irr}(t_b)$ rather than to the time-dependent magnetization. Since the variation in M_{irr} during the relaxation measurement is small, the error introduced is also small.[49] Before discussing the physics that U^* would reveal, we discuss next the relationship between this apparent activation energy, which is experimentally accessible, and the actual activation energy.

The actual activation energy U is a rather complex quantity involving not only a term due to the microscopic interaction between the flux lines and the pinning centers U_{int}, but also an extrinsic dependence on the distribution of the critical current density.[50] Miu *et al.*[51] inferred that

$$U=U_{int}(J)\ln(J_c/J). \quad (4)$$

Then, the relationship between U^* and U, hence U_{int}, can be obtained through the general dependence $U=k_BT\ln(t/t_0)$ (Ref. 52) along with Eqs. (2) and (4) (see the Appendix for more details) as

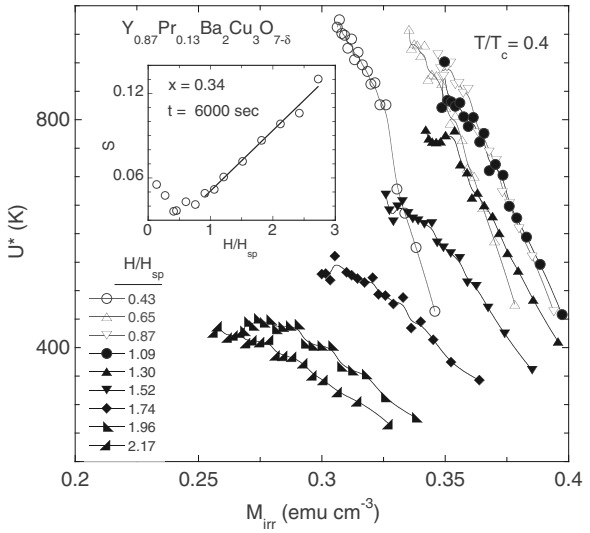

FIG. 5. Plot of the apparent activation energy U^*, obtained from relaxation measurements, vs irreversible magnetization M_{irr} of an $Y_{0.87}Pr_{0.13}Ba_2Cu_3O_{7-\delta}$ single crystal measured at different applied magnetic fields and at the reduced temperature $T/T_c \approx 0.4$. Empty and filled symbols are for $H < H_{sp}$ and $H > H_{sp}$, respectively. Solid lines are a guide for the eye. Inset: Field dependence of the relaxation rate S measured at a time $t \approx 6000$ s.

$$U^*(J,H) = U_{int}(J) - J\frac{dU_{int}}{dJ}\ln\left(\frac{J_c}{J}\right). \tag{5}$$

Therefore, U^* is always an overestimate of U_{int} since dU_{int}/dJ is negative. Nevertheless, Eq. (5) shows that the approximation of U_{int} with U^* is valid as long as the current density is close to J_c and it breaks down for $J \ll J_c$, i.e., for $H \gg H_{sp}$. Thus, a plot of $U^*(J)$ determined from Eq. (2) with S obtained from the relaxation data in the regime where J is not too far from J_c, i.e., for not extremely long relaxation times and for magnetic fields around H_{sp}, gives an accurate information on U_{int} and, hence, on the evolution of the vortex matter when the temperature and magnetic field are swept.

The plot of U^* vs M_{irr} ($M_{irr} \propto J$) is shown in Fig. 5 for the $x=0.13$ single crystal measured at $T/T_c \approx 0.4$ and for different values of the reduced field H/H_{sp}. The different evolutions of the activation energy below and above H_{sp} are salient. Specifically, for fields smaller than H_{sp} (open symbols), $U^*(J,H)$ rapidly increases as the current J (or, equivalently, M_{irr}) decreases, which is an expected behavior for an elastic vortex system in the collective pinning regime. Above H_{sp} (filled symbols), the increase in U^* with decreasing current density becomes slower and slower, which suggests a smooth crossover at H_{sp} to another regime, most likely a regime dominated by the fast proliferation of dislocations.

We have observed a similar behavior of $U^*(J)$ for all Pr concentrations studied. However, for the same reduced field range and for $T/T_c \approx 0.4$, the range of values of U^* decreases with increasing Pr concentration, e.g., U^* varies between 200 and 1000 K for $x=0.13$, 100–600 K for $x=0.34$, and 50–400 K for $x=0.47$. The decrease in the range of U^* with increasing x is in agreement with previous results on $Y_{1-x}Pr_xBa_2Cu_3O_{7-\delta}$ polycrystalline pellets.[53]

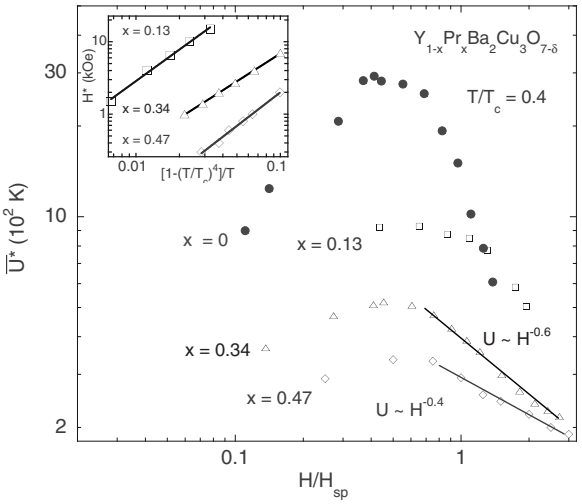

FIG. 6. Log-log plot of the field H dependence of the average activation energy $\bar{U}^*$ of $Y_{1-x}Pr_xBa_2Cu_3O_{7-\delta}$, $x=0$ (Ref. 36), 0.13, 0.34, and 0.47 single crystals, measured at a reduced temperature $T/T_c=0.4$. The lines are fits of the data with a power law. Inset: Temperature dependence of $H^*(T)$ as determined from the minima of $S(H)$.

As a function of field, U^* [or, equivalently, S; see Eq. (2)] systematically shows, at any relaxation time t, a maximum (minimum) at a field H^*, which is between H_{on} and H_{sp} [see, for example, the inset of Fig. 5 for $S(H)$ for the $x=0.34$ single crystal]. Therefore, the slowest magnetic relaxation takes place at a field value just below H_{sp} and not at H_{sp}. At fields higher than H^*, $S(H)$ increases almost linearly.

The apparent activation energy U^* is a nonlinear function of time, increasing as the current density relaxes to lower values. However, a reliable estimate of its overall field dependence over a reasonable time window from t_1 to t_2 can be obtained by replacing the derivative in Eq. (2) with finite differences. This average apparent activation energy $\bar{U}^*$ is given by

$$\bar{U}^*(H) = k_B T \ln\left(\frac{t_2}{t_1}\right)\frac{M_{irr}(t_b,H)}{\Delta M_{irr}(H)}, \tag{6}$$

where $\Delta M_{irr}(H) = M_{irr}(H,t_1) - M_{irr}(H,t_2)$. Figure 6 is a log-log plot of $\bar{U}^*(H)$, as extracted from relaxation measurements over the time window 600 s $\leq t \leq$ 4000 s, for three Pr concentrations ($x=0.13$, 0.34, and 0.47) and for an $x=0$ single crystal taken from the literature,[37] with U^* determined from Eq. (2) at 1000 s. This figure does not give the H dependence of the barrier at fixed current density since J also changes with field. Nevertheless, its advantage is that it gives an explicit dependence of the barrier on H, which facilitates the identification of the creep regime and the comparison between samples with different charge carrier densities. $\bar{U}^*(H)$ displays again a maximum at H^*. The relative difference $(H_{sp}-H^*)/H_{sp}$ between H^* and H_{sp} is maximum for the $x=0.34$ single crystal, for which the value of the second magnetization peak is enhanced (see Fig. 2). For $H < H^*$, $\bar{U}^*$ increases with increasing magnetic field, which is consistent

with the elastic (collective) creep mechanism. For $H>H^*$, $\bar{U}^*(H)$ decreases roughly as a power law with increasing H, i.e., $\bar{U}^*(H)\propto H^{-\nu}$, with $\nu=0.6$ and 0.4 for the $x=0.34$ and 0.47 single crystals, respectively, which indicates plastic vortex creep,[3] and a more abrupt drop for the $x=0$ and 0.13 single crystals. A simple model for plastic pinning[2] yields an exponent $\nu=0.5$, while other reports give $\nu=0.55$ for $Bi_2Sr_2CaCu_2O_8$,[54] $\nu=0.7$ for $YBa_2Cu_3O_{7-\delta}$,[2] and $HgBa_2CuO_{4+\delta}$,[55] and $\nu\approx 1$ for $Tl_2Ba_2CaCu_2O_8$.[56] Hence, as expected, these $\bar{U}^*(H)$ data are consistent with the $U^*(J,H)$ data of Fig. 5, but, additionally, they give the quantitative dependence of the activation energy on the magnetic field. Based on these data, we also conclude that, at least in the case of Pr-doped $YBa_2Cu_3O_{7-\delta}$, the order-disorder crossover is best given by $H^*(T)$ ($H_{on}<H<H_{sp}$), even though, as discussed above, the two characteristic fields H_{on} and H_{sp} are the ones that have been previously related to the order-disorder transition.

Based on our above conclusion, leveling the elastic and plastic energies engaged in the equilibrium of the flux lines, i.e., $U_{el}=U_{pl}$, at H^* gives $H^*\propto 1/T^2\lambda^4\propto[\{1-(T/T_c)^4\}/T]^\chi$, with $\chi=2$. The fit of H^* vs $[1-(T/T_c)^4]/T$ for $0.3\leqslant T/T_c\leqslant 0.8$ is shown as a log-log plot in the inset of Fig. 6. The values of the exponent χ are 1.44, 1.27, and 1.54 for the $x=0.13$, 0.34, and 0.47 single crystal, respectively. The good fit of the data with the above expression supports our conclusion that the elastic to plastic crossover takes place at H^*. It is interesting to note that the exponents are nonmonotonic with increasing x, with the lowest value for the $x=0.34$ sample.

Since, as shown above, the activation energy is a function of current density, temperature, and magnetic field [see Eq. (3)], changes in any one of these parameters drive continuously the vortex matter into different elastic and plastic creep regimes. Hence, magnetic relaxation data give information about a specific flux-creep regime for a given T and H through the critical exponent $\mu(T,H)$ present in Eq. (1). A fit of the M_{irr} vs $\ln t$ data with Eq. (1) for different T and H gives $\mu(T,H)$.

Figure 7 and its insets are plots of $\mu(T,H)$ for different charge carrier densities, i.e., Pr doping. Note that $\mu(H)$ displays a peak at the same magnetic field value H^* at which $\bar{U}^*(H)$ is maximum. Therefore, as discussed above, the elastic pinning mechanism dominates for $H_{on}<H<H^*$, while the plastic mechanism dominates for $H>H^*$. Also, note that μ decreases with increasing temperature and decreasing charge carrier density (increasing x).

The collective (elastic) creep theory[26] predicts that $\mu=1/7$ for single vortex creep (at high current and low field), $\mu=5/2$ for small vortex-bundle creep (at intermediate current and field), $\mu=1$ for the creep of intermediate vortex bundles, and $\mu=7/9$ for the creep of large vortex bundles (at low current and high field). As the data show, $\mu(H)$ does not exactly follow these theoretical predictions in the regime where flux lines are expected to behave elastically, i.e., for $H_{on}<H<H^*$. For example, $\mu>2$ but smaller than 2.5 for the lowest measured temperature ($T/T_c=0.3$) even in the case of the $x=0.13$ single crystal, which is expected to have the strongest elastic response. Hence, although these values

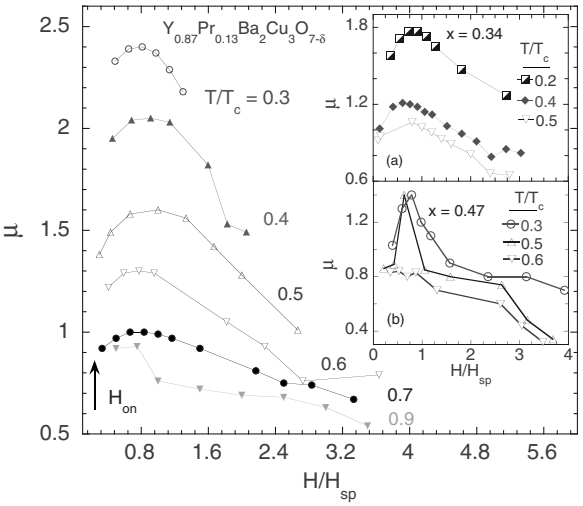

FIG. 7. Field H dependence of the relaxation exponent μ of an $Y_{0.87}Pr_{0.13}Ba_2Cu_3O_{7-\delta}$ single crystal measured at different reduced temperatures ($T_c=82$ K). Insets: The same plot for the (a) $Y_{0.66}Pr_{0.34}Ba_2Cu_3O_{7-\delta}$ single crystal ($T_c=50$ K) and (b) $Y_{0.53}Pr_{0.47}Ba_2Cu_3O_{7-\delta}$ single crystal ($T_c=34$ K).

indicate that the relaxation of the flux vortices is mainly due to the creep of small vortex bundles, the admixture of the plastic contribution limits μ to values smaller than 2.5. Similar deviations from the theoretical exponents for plastic creep[22] are clear for $H>H^*$.

The direct (inverse) correlation between the values of the creep exponent μ and the charge carrier density (Pr doping) as well as the decrease in the value of μ with increasing T (see Fig. 7 and its insets) reflects the decreased role of the vortex lattice properties over a single vortex behavior with decreasing n_s or increasing T as a result of the weakening of the elastic moduli with decreasing n_s [$C_{66}\propto\lambda^{-2}\propto n_s(x)$] or increasing T. As a consequence, the crossover magnetic field H_{sb} from single vortex to small bundle collective pinning increases with decreasing n_s (increasing x) or increasing T since $H_{sb}\propto\lambda^{8/3}\propto n_s^{-4/3}$.[26] Hence, H_{sb} cannot be reached in strongly underdoped single crystals before the full crossover to plastic pinning. This explains the decrease in the value of the exponent μ at H^* in Fig. 7 and its insets with increasing x or T.

For magnetic fields higher than H^*, μ decreases monotonically with increasing H. However, the value of $\mu=10/21$, which is representative of the plastic creep of the lattice, is accessible only at high temperatures. At lower T, one needs magnetic fields higher than the one available (5 T) in order to be able to detect this regime. Additionally, the elastic contributions do not vanish completely in the plastic regime.[46]

IV. SUMMARY

In summary, we investigated the evolution of the SMP with the charge carrier density by an appropriate doping that avoids the change in the quenched disorder in a sensitive way. For this goal, we carried out magnetization and magnetic relaxation measurements on a series of

$Y_{1-x}Pr_xBa_2Cu_3O_{7-\delta}$ single crystals, in which the concentration of Pr ions controls the charge carrier density $n_s(x)$. We have found that the quenched disorder is necessary for the existence of irreversibility and of the SMP, but the principal ingredient that controls the evolution of the vortex matter through different regimes is the charge carrier density. Specifically, we have found that the SMP is broad and its magnitude is nonmonotonic with the amount of doping: it increases with decreasing charge carrier density up to a doping at around $x=0.34$ followed by a decrease with a further decrease in n_s (increasing Pr concentration). The two characteristic magnetic fields, the onset field H_{on} and the field H_{sp} corresponding to the SMP, decrease with increasing temperature T, but they follow different T dependences: $H_{on} \propto T^{\nu_{on}}$ while $H_{sp} \propto [1-(T/T_c)^2]^{\nu_{sp}}$, with the exponent ν_{sp} following the same nonmonotonic trend as a function of n_s as H_{sp}. Within the collective creep theory, we determined the apparent activation energy. Its evolution with J has shown that the vortex system is predominantly elastically pinned below H_{sp}, while above H_{sp}, there is a smooth crossover to a vortex regime most likely dominated by the proliferation of dislocations. The field dependence of the average apparent pinning potential $\bar{U}^*$ displays a maximum at a magnetic field H^*, with $H_{on} < H^* < H_{sp}$, which is consistent with the presence of an elastic (collective) creep mechanism at low fields and a plastic vortex creep at high H values. The transition from the Bragg glass to the dislocation-rich vortex system gradually occurs and extends on a rather large field range. For this reason, we propose that the order-disorder line must be defined by the maximum of the average activation energy, which is located at H^*, below H_{sp} but above the inflection point of the $M(H)$ curves.

ACKNOWLEDGMENTS

This research was supported by the National Science Foundation under Grant No. DMR-0705959 at KSU, the U.S. Department of Energy under Grant No. DE-FG02-04ER46105 at UCSD, and the NASR under Grant No. CEX 45/2006 at NIMP.

APPENDIX

As mentioned in the main text, Miu *et al.*[51] inferred the following current dependence of the activation energy:

$$U(J) = U_{int}(J)\ln\left(\frac{J_c}{J}\right).$$

Then,

$$\frac{dU}{dJ} = \frac{dU_{int}}{dJ}\ln\left(\frac{J_c}{J}\right) + U_{int}\frac{d(\ln J_c - \ln J)}{dJ}$$
$$= \frac{dU_{int}}{dJ}\ln\left(\frac{J_c}{J}\right) - \frac{U_{int}}{J},$$

or

$$-J\left(\frac{dU}{dJ}\right) = U_{int} - J\frac{dU_{int}}{dJ}\ln\left(\frac{J_c}{J}\right). \tag{A1}$$

As shown by Eq. (2), the normalized relaxation rate is

$$-\frac{1}{M_{irr}(t)}\frac{dM_{irr}(t)}{d\ln(t)} = \frac{k_BT}{U^*(J,T,H)}. \tag{A2}$$

Also, the actual activation energy is[52]

$$U = k_BT\ln(t/t_0),$$

which can be written as

$$\frac{dU}{d\ln t} = k_BT. \tag{A3}$$

Since $M_{irr} \propto J$, Eq. (A2) becomes

$$-\frac{1}{J}\frac{dJ}{d\ln t} = \frac{dU}{d\ln t}\frac{1}{U^*};$$

hence,

$$U^* = -J\frac{dU}{dJ}. \tag{A4}$$

By using Eq. (A1), the above equation gives

$$U^* = -J\frac{dU}{dJ} = U_{int} - J\frac{dU_{int}}{dJ}\ln\left(\frac{J_c}{J}\right).$$

*Permanent address: National Institute of Materials Physics, 077125 Bucharest-Magurele, Romania.

[1] A. A. Zhukov, H. Küpfer, G. Perkins, L. F. Cohen, A. D. Caplin, S. A. Klestov, H. Claus, V. I. Voronkova, T. Wolf, and H. Wühl, Phys. Rev. B **51**, 12704 (1995).
[2] Y. Abulafia, A. Shaulov, Y. Wolfus, R. Prozorov, L. Burlachkov, Y. Yeshurun, D. Majer, E. Zeldov, H. Wühl, V. B. Geshkenbein, and V. M. Vinokur, Phys. Rev. Lett. **77**, 1596 (1996).
[3] D. Giller, A. Shaulov, R. Prozorov, Y. Abulafia, Y. Wolfus, L. Burlachkov, Y. Yeshurun, E. Zeldov, V. M. Vinokur, J. L. Peng, and R. L. Greene, Phys. Rev. Lett. **79**, 2542 (1997).
[4] M. Jirsa, L. Půst, D. Dlouhý, and M. R. Koblischka, Phys. Rev. B **55**, 3276 (1997).
[5] M. Reissner and J. Lorenz, Phys. Rev. B **56**, 6273 (1997).
[6] H. Küpfer, Th. Wolf, C. Lessing, A. A. Zhukov, X. Lançon, R. Meier-Hirmer, W. Schauer, and H. Wühl, Phys. Rev. B **58**, 2886 (1998).
[7] J. T. Manson, J. Giapintzakis, and D. M. Ginsberg, Phys. Rev. B **54**, 12517 (1996).
[8] S. Kokkaliaris, P. A. J. de Groot, S. N. Gordeev, A. A. Zhukov, R. Gagnon, and L. Taillefer, Phys. Rev. Lett. **82**, 5116 (1999).
[9] N. Avraham, B. Khaykovich, Y. Myasoedov, M. Rappaport, H. Shtrikman, D. E. Feldman, T. Tamegai, P. H. Kes, M. Li, M. Konczykowski, K. V. D. Beek, and E. Zeldov, Nature (London) **411**, 451 (2001).
[10] Y. P. Sun, W. H. Song, J. J. Du, and H. C. Ku, Phys. Rev. B **66**,

104520 (2002).
[11] L. Miu, S. Popa, V. Sandu, T. Noji, Y. Koike, D. Miu, S. Diaz, and G. Chouteau, Phys. Rev. B **70**, 134523 (2004).
[12] D. Ertas and D. R. Nelson, Physica C **272**, 79 (1996).
[13] V. Vinokur, B. Khaykovich, E. Zeldov, M. Konczykowski, R. A. Doyle, and P. H. Kes, Physica C **295**, 209 (1998).
[14] A. E. Koshelev and V. M. Vinokur, Phys. Rev. B **57**, 8026 (1998).
[15] T. Nishizaki, T. Naito, and N. Kobayashi, Phys. Rev. B **58**, 11169 (1998).
[16] K. Shibata, T. Nishizaki, M. Maki, and N. Kobayashi, Phys. Rev. B **72**, 014525 (2005).
[17] K. Watanabe, T. Kita, and M. Arai, Phys. Rev. B **71**, 144515 (2005).
[18] Y. Radzyner, A. Shaulov, and Y. Yeshurun, Phys. Rev. B **65**, 100513(R) (2002).
[19] A. I. Larkin and V. M. Vinokur, Phys. Rev. Lett. **75**, 4666 (1995).
[20] G. I. Menon, Phys. Rev. B **65**, 104527 (2002); S. S. Banerjee, A. K. Grover, M. J. Higgins, G. I. Menon, P. K. Mishra, D. Pal, S. Ramakrishnan, T. V. Chandrasekhar Rao, G. Ravikumar, V. C. Sahni, S. Sarkar, and C. V. Tomy, Physica C **355**, 39 (2001).
[21] P. Moretti, M. Carmen Miguel, M. Zaiser, and S. Zapperi, Phys. Rev. Lett. **92**, 257004 (2004).
[22] J. Kierfeld, H. Nordborg, and V. M. Vinokur, Phys. Rev. Lett. **85**, 4948 (2000).
[23] U. Divakar, A. J. Drew, S. L. Lee, R. Gilardi, J. Mesot, F. Y. Ogrin, D. Charalambous, E. M. Forgan, G. I. Menon, N. Momono, M. Oda, C. D. Dewhurst, and C. Baines, Phys. Rev. Lett. **92**, 237004 (2004).
[24] G. I. Menon, A. Drew, U. K. Divakar, S. L. Lee, R. Gilardi, J. Mesot, F. Y. Ogrin, D. Charalambous, E. M. Forgan, N. Momono, M. Oda, C. Dewhurst, and C. Baines, Phys. Rev. Lett. **97**, 177004 (2006).
[25] W. J. Padilla, Y. S. Lee, M. Dumm, G. Blumberg, S. Ono, K. Segawa, S. Komiya, Y. Ando, and D. N. Basov, Phys. Rev. B **72**, 060511(R) (2005).
[26] G. Blatter, M. V. Feigel'man, V. B. Geshkenbein, A. I. Larkin, and V. M. Vinokur, Rev. Mod. Phys. **66**, 1125 (1994).
[27] G. P. Mikitik and E. H. Brandt, Phys. Rev. B **64**, 184514 (2001).
[28] J. Kierfeld and V. Vinokur, Phys. Rev. B **69**, 024501 (2004).
[29] J. D. Jorgensen, B. W. Veal, A. P. Paulikas, L. J. Nowicki, G. W. Crabtree, H. Claus, and W. K. Kwok, Phys. Rev. B **41**, 1863 (1990).
[30] M. Baziljevich, D. Giller, M. McElfresh, Y. Abulafia, Y. Radzyner, J. Schneck, T. H. Johansen, and Y. Yeshurun, Phys. Rev. B **62**, 4058 (2000).
[31] R. Fehrenbacher and T. M. Rice, Phys. Rev. Lett. **70**, 3471 (1993).
[32] A. I. Liechtenstein and I. I. Mazin, Phys. Rev. Lett. **74**, 1000 (1995).
[33] R. P. S. M. Lobo, E. Ya. Sherman, D. Racah, Y. Dagan, and N. Bontemps, Phys. Rev. B **65**, 104509 (2002).
[34] C. N. Jiang, A. R. Baldwin, G. A. Levin, T. Stein, C. C. Almasan, D. A. Gajewski, S. H. Han, and M. B. Maple, Phys. Rev. B **55**, R3390 (1997).
[35] L. M. Paulius, B. W. Lee, M. B. Maple, and P. K. Tsai, Physica C **230**, 255 (1994).
[36] M. Oussena, P. A. J. de Groot, A. Marshall, and J. S. Abell, Phys. Rev. B **49**, 1484 (1994).
[37] M. Pissas, E. Moraitakis, G. Kallias, and A. Bondarenko, Phys. Rev. B **62**, 1446 (2000).
[38] D. Pal, S. Ramakrishnan, A. K. Grover, D. Dasgupta, and B. K. Sarma, Phys. Rev. B **63**, 132505 (2001).
[39] V. Sandu, P. Gyawali, T. Katuwal, C. C. Almasan, B. J. Taylor, and M. B. Maple, Phys. Rev. B **74**, 184511 (2006).
[40] Y. M. Wang, M. S. Fuhrer, A. Zettl, S. Ooi, and T. Tamegai, Phys. Rev. Lett. **86**, 3626 (2001).
[41] B. Kalisky, D. Giller, A. Shaulov, T. Tamegai, and Y. Yeshurun, Phys. Rev. B **72**, 014531 (2005).
[42] H. Küpfer, A. Will, R. Meier-Hirmer, Th. Wolf, and A. A. Zhukov, Phys. Rev. B **63**, 214521 (2001).
[43] C. J. Olson, C. Reichhardt, and F. Nori, Phys. Rev. Lett. **81**, 3757 (1998).
[44] B. Kalisky, Y. Bruckental, A. Shaulov, and Y. Yeshurun, Phys. Rev. B **68**, 224515 (2003).
[45] A. Pautrat, C. Simon, C. Goupil, P. Mathieu, A. Brulet, C. D. Dewhurst, and A. I. Rykov, Phys. Rev. B **75**, 224512 (2007).
[46] M. Chandran, R. T. Scalettar, and G. T. Zimányi, Phys. Rev. B **69**, 024526 (2004).
[47] K. Deligiannis, P. A. J. de Groot, M. Oussena, S. Pinfold, R. Langan, R. Gagnon, and L. Taillefer, Phys. Rev. Lett. **79**, 2121 (1997).
[48] T. Nishizaki, T. Naito, S. Okayasu, A. Iwase, and N. Kobayashi, Phys. Rev. B **61**, 3649 (2000).
[49] Y. Yeshurun, A. P. Malozemoff, and A. Shaulov, Rev. Mod. Phys. **68**, 911 (1996).
[50] J. Z. Sun, C. B. Eom, B. Lairson, J. C. Bravman, and T. H. Geballe, Phys. Rev. B **43**, 3002 (1991).
[51] L. Miu, T. Noji, Y. Koike, E. Cimpoiasu, T. Stein, and C. C. Almasan, Phys. Rev. B **62**, 15172 (2000).
[52] M. V. Feigel'man, V. B. Geshkenbein, A. I. Larkin, and V. M. Vinokur, Phys. Rev. Lett. **63**, 2303 (1989).
[53] L. M. Paulius, C. C. Almasan, and M. B. Maple, Phys. Rev. B **47**, 11627 (1993).
[54] L. Miu, E. Cimpoiasu, T. Stein, and C. C. Almasan, Physica C **334**, 1 (2000).
[55] M. Pissas, D. Stamopoulos, E. Moraitakis, G. Kallias, D. Niarchos, and M. Charalambous, Phys. Rev. B **59**, 12121 (1999).
[56] P. Chowdhury, H.-J. Kim, I. S. Jo, and S. I. Lee, Phys. Rev. B **66**, 184509 (2002).